Journal of Nuclear Materials 519 (2019) 265–273

Contents lists available at ScienceDirect

Journal of Nuclear Materials

journal homepage: www.elsevier.com/locate/jnucmat

Solute precipitation on a screw dislocation and its effects on dislocation mobility in bcc Fe

M.I. Pascuet [a, *], G. Monnet [b], G. Bonny [c], E. Martínez [d], J.J.H. Lim [e], M.G. Burke [f], L. Malerba [c, 1]

[a] Materials Department, CONICET-CNEA, Godoy Cruz, 2290, C1425FQB, CABA, Argentina
[b] EDF – R&D, MMC, Avenues des Renardières, 77680, Moret sur Loing, France
[c] Nuclear Materials Science Institute, SCK•CEN, Boeretang 200, 2400, Mol, Belgium
[d] Material Science and Technology Division, MST-8, Los Alamos National Laboratory Los Alamos, 87545, NM, USA
[e] Materials Science and Scientific Computing Department, United Kingdom Atomic Energy Authority, Culham Science Centre, Abingdon, OX14 3DB, United Kingdom
[f] Materials Performance Centre, The University of Manchester, Manchester, M13 9PH, United Kingdom

ARTICLE INFO

Article history:
Received 17 September 2018
Received in revised form
11 March 2019
Accepted 2 April 2019
Available online 3 April 2019

Keywords:
Iron alloys
Segregation
Screw dislocation mobility
Monte Carlo

Disloations a atoms segregation

ABSTRACT

Reactor pressure vessel steels are well-known to harden and embrittle under neutron irradiation. The primary mechanism of radiation embrittlement for these bainitic steels is the obstruction of dislocation motion, mainly due to clusters or precipitates of solute atoms such as Cu, Ni, Mn, Si and P. Microstructural examinations reveal that these clusters or precipitates are often preferentially formed at dislocation lines, which are sometimes completely surrounded by segregated solute clusters. Evidence of this is provided in this work, too, which extends a previous one dedicated to edge dislocations, by studying the effect of this segregation around screw dislocations (Burgers vector $\mathbf{b} = 1/2$ [111]) on the critical stress for dislocation motion. A Monte Carlo algorithm in a variance-constrained semi-grand canonical (VC-SGC) ensemble is applied to study the decoration of atoms around dislocations, by minimizing the free energy. Next, the critical stress for dislocation unpinning from the clusters is evaluated by standard molecular dynamics to analyze the effect of Cu, Ni, Mn, and P segregation in the Fe matrix. Consistently with expectations and in agreement with previous work, our results highlight that the required stress for triggering dislocation motion drastically increases due to the presence of segregated solutes. Our finding is that solute-decorated screw dislocations may be considered as practically immobile because of the strong segregation around them.

1. Introduction

Radiation-induced hardening and embrittlement in reactor pressure vessel (RPV) steels is one of the main limiting factors for the lifetime of nuclear power plants. The primary mechanism of embrittlement is, at the mesoscopic scale, the obstruction of the dislocation motion by structural defects created during irradiation. Experimental techniques such as small angle neutron scattering (SANS) and atom probe tomography (APT) evidenced the massive presence, in irradiated RPV steels, of precipitates rich in Cu, Mn, Ni, Si and P [1]. Recently, also Scanning Transmission Electron Microscopy & Electron Energy Loss Spectroscopy (STEM-EELS) provided clear evidence of the formation of precipitates of this type. Both APT [2,3] and STEM-EELS studies [4,5] showed in particular evidence of segregation of these solutes in the vicinity of dislocations, either with formation of discrete precipitates, or in a uniform way. The dislocation motion is thus expected to be reduced or even impeded by this enrichment, causing hardening and contributing to loss of ductility.

Loss of ductility due to dislocation pinning on precipitates

The computing capabilities nowadays available enable advanced atomistic modelling techniques to be extensively used to complement and support experimental results. In a previous work [6], solute segregation and precipitation near an edge dislocation was studied using computational methods. There, the accumulation of solutes at an edge dislocation in a bcc Fe matrix containing different

* Corresponding author.
E-mail address: pascuet@cnea.gov.ar (M.I. Pascuet).
[1] Current affiliation: Centro de Investigaciones Energéticas, Medioambientales y Tecnológicas (CIEMAT), División de Materiales de Interés Energético, Avda. Complutense 40, 28040 Madrid (Spain).

https://doi.org/10.1016/j.jnucmat.2019.04.007
0022-3115/

proportions of Cu, Ni, Mn and P was simulated using an atomistic Metropolis Monte Carlo (MMC) method in the variance-constrained semi-grand canonical (VC-SGC) ensemble, with interatomic potentials built in such a way to accurately reproduce the thermodynamic properties of the relevant systems [7,8]. The results were consistent with those of Bonny et al. [9], obtained using similar but non-coincident MMC techniques, in terms of ranges where precipitation and segregation are thermodynamically favoured. As will be seen, these results are also in striking agreement with experimental observations. Next, the effect of the solute segregation on the mobility of edge dislocations was studied [6], finding that the stress necessary to set the dislocation in motion increased tremendously compared with pure Fe [10] and suggesting that decorated edge dislocations are most likely immobilized. The shear resistance of the precipitates was found to be close to 2.4 GPa at room temperature.

In the present work the role played by solute segregation on the mobility of screw dislocations is studied. In the literature, a somewhat similar work has been performed for the Fe-C case [11]. Traditionally, however, atomistic studies investigated how precipitates found in the matrix are sheared by moving dislocations, generally limiting the study to edge types [12–15]. In contrast, the effect of initial decoration on dislocation mobility, before their motion is triggered by the application of external stress, is not commonly investigated [11,16]. For this reason, in this work we exclusively focus on the case in which the solutes accumulate near the dislocation line, before load is applied, considering the case of the screw dislocation. This piece of information is of high importance for dislocation dynamics simulations, in order to assess the precipitate shear resistance to the new dislocations generated by deformation.

To simulate these effects in the case of screw dislocation dipoles, boxes containing several hundreds of thousands of atoms, i.e., substantially larger than in the edge dislocation case, are necessary, to avoid the interaction of the screw dipole and thus its annihilation. Therefore, the use of a massively parallel code is required. As in our previous work, we use a combination of Metropolis Monte Carlo (MMC) and molecular dynamics (MD), as implemented in LAMMPS [17]. Firstly, we estimated the full phase boundary versus temperature and solute content, as described by the interatomic potentials used [7,8], in small simulation boxes containing a single screw dislocation, by means of exchange Monte Carlo at fixed composition, in the isothermal-isobaric ensemble. The solute segregation configurations in thermal equilibrium near a screw dislocation dipole, later usable to apply an external load, were subsequently obtained in much larger volumes, using the more efficient Monte Carlo (MC) method in the variance-constrained semi-grand-canonical (VC-SGC) ensemble [18]. A direct comparison of the results with STEM-EELS observations is made. Both MC methods, lead to equivalent results. In both cases the thermal vibrations are sampled using MD, which is computationally more efficient, thereby corresponding to a hybrid MD-MC method. Given the solute segregated configurations from the VC-SGC simulations, classical MD is then applied at various temperatures to obtain stress-strain curves of the MD simulation box.

In the next section the computational models and the experimental technique are described. The results are presented in Section 3, distinguishing three case studies according to the material, FeNiMn, FeCuNiMn or FeP. Section 4 is devoted to discussion; summary and conclusions are given in Section 5.

2. Methods

2.1. Solubility limits

The phase stability boundaries in the presence of a screw dislocation were obtained as described in Ref. [9], by applying an exchange Monte Carlo method in the isothermal-isobaric (NPT) ensemble, scanning temperatures on a 50 K grid for different fixed compositions, namely varied between 0.5 and 2 at.% for Ni and Mn in equimolar fractions, while the Cu content (when present) was fixed to 0.5 at.%. For each temperature and composition, the solutes were initially randomly distributed in a matrix of Fe atoms, contained in simulation volumes with dimensions 4.9 x $14.0 \times 16.1\ \mathrm{nm}^3$, which corresponds to approximately $96{\cdot}10^3$ atoms. After thermalization via MD in the NPT ensemble for 5 ps, the atomic chemical species were rearranged by applying the exchange Monte Carlo, as implemented in LAMMPS, using the EAM interatomic potential proposed by Bonny et al. [7]. Then the hybrid exchange MC using MD to simulate the NPT ensemble was performed and convergence of each simulation was reached in 4 10^6 MC steps. For each possible pair of atom types, 100 exchanges were performed every 50 MD steps. In this way the phase stability boundary was promptly established by visual inspection of precipitation in the converged simulation boxes.

The simulation box axes were oriented along the [111], [1$\bar{1}$2] and [$\bar{1}$10] directions. A ½⟨111⟩ screw dislocation was introduced at the center of the box along the [111] direction. Standard periodic boundary conditions were applied along *x* and *y* directions and free surfaces on the top and bottom *z* planes. The resulting box is skewed, with an extra component along *y* of size + b/2. To avoid possible solute clustering on the free surfaces, the exchange of atoms was only allowed in the center slab of the box, about 1 nm from the free surfaces. The inner slab contained 81 10^3 atoms that are subjected to exchange MC. This set-up was preferred over the dipole for the solubility limit study, to allow a smaller simulation volume to be used.

2.2. Solute enrichment

For the second part of the work a somewhat different approach was used, in order to get relevant reference configurations to study the mobility of solute decorated screw dislocations. Solute precipitation via minimization of the free energy of the system was simulated by an MD-MC hybrid algorithm in the VC-SGC ensemble [18]. This method is suitable to efficiently simulate systems with millions of particles in the whole concentration range. Chemical mixing, precipitation, relaxation and thermal vibrations, as described by the interatomic potentials, are taken into account by the combination between transmutation moves and MD steps. In the SGC ensemble the phases inside the miscibility gap have identical chemical potentials and therefore the concentration cannot be held constant. Outside the miscibility gap, the chemical potential defines the equilibrium concentration. The method is explained in Ref. [6], where solute segregation near an edge dipole was studied. The only difference with respect to the present case is the type of dislocation and the larger size of the simulation volume. The interaction for ternary FeNiMn and quaternary FeCuNiMn systems are modelled using the same EAM interatomic potential as in the preliminary phase boundary study [7].

The box containing the screw dipole was generated using linear elasticity [19] in a crystallite with the normal axes *x*, *y* and *z* oriented as the [1$\bar{1}$0], [$\bar{1}\bar{1}$2] and [111] directions, that contain approximately 1.9 10^6 bcc Fe atoms. The Burgers vectors of the dipole are $\mathbf{b}_1 = a_0/2$ [111] and $\mathbf{b}_2 = -a_0/2$ [111], where a_0 is the lattice parameter of Fe [7]. Since $\mathbf{b_1}$ and $\mathbf{b_2}$ have opposite signs, periodicity can now also be recovered along the [1$\bar{1}$0] direction, leading to periodic boundary conditions in all three directions. However, as in the previous section, the box is non-orthogonal. The dimensions of the box are $35 \times 65 \times 10\ \mathrm{nm}^3$ and are sufficient to ensure that the dislocation lines, both lying along the [111]

direction, are well-separated from each other, so as to prevent their mutual interactions. The $\Delta\mu$ values used to trigger segregation and precipitation are: −0.69 for Cu, 0.29 for Ni, −1.38 for Mn and −2.5 for P, with $\kappa = 1000$ in all cases [6]. These values have been identified to drive the system correctly into the miscibility gap, also by comparison with the method described in 2.1, and constrain it to sample configurations with the required concentration in each case. Once these values are fixed, 500 MD steps are performed between MC steps, decreasing the free energy of the system to achieve the desired concentrations: 1%Ni-1%Mn, 0.7%Ni-1.4%Mn, 0.5%Cu-1%Ni-1%Mn, 0.5%Cu-0.7%Ni-1.4%Mn and, in the case of P up to 1.64 10^{-2}%. The temperatures considered were: 300, 400 and 500 K (i.e., from ambient temperature to a temperature right below the operating temperature of nuclear reactors). These initial compositions were chosen for consistency with the work done on edge dislocations [6] and correspond to the solute content of RPV steels, representative of those used in nuclear power plants.

2.3. Stress-strain curves

Once the equilibrium configurations were obtained, the box was cut in two parts, each containing one of the two dislocations of the dipole, as depicted in Fig. 1. Classical MD is applied in one of these parts to get the stress-strain curves. Simple shear strain is applied at a constant strain rate ($10^8 s^{-1}$ or $10^9 s^{-1}$, depending on the amount of solutes around the dislocation core) at 300 and 600 K, corresponding to typical tensile test temperatures in the case of RPV steels. The corresponding dislocation density is 8.8 10^{14} m^{-2}. To apply the shear strain, two atomic layers of 12 Å thickness, normal to the *y* axis, are fixed, as shown in Fig. 1. Periodic boundary conditions are applied along the [111] and $[1\bar{1}0]$ directions. Shear strain is applied by displacing the left side of the simulation box in the direction of the Burgers vector, *z*, and the corresponding resolved shear stress induced by the applied deformation is calculated as $\sigma_{xz} = F_z/A_{xz}$, where F_z is the total force in the *z* direction and A_{xz} is the *xz* cross section area [20].

2.4. Electron microscopy characterisation

The STEM-EELS imaging was performed simultaneously to study the MnNiCu solute clusters induced in an RPV steel after irradiation [21]. In this study, a spherical aberration-corrected FEI Titan G2 0–200 with Super X EDX (ChemiSTEM™) operated at 200 kV and equipped with a GIF Quantum 965 EELS has been used to provide independent compositional analyses of the nano-scale solute clusters that form during irradiation.

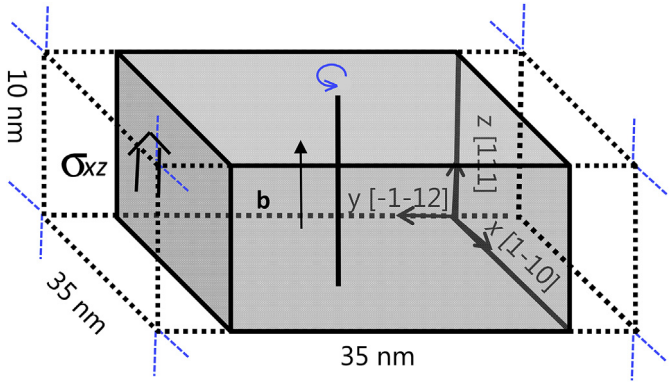

Fig. 1. Schematic representation of box containing screw dislocation with b = [111].

3. Results

3.1. Solubility curves and precipitated phases

In Fig. 2, the NiMn and CuNiMn solubility limits in presence of a screw dislocation is compared to the equilibrium one taken from Bonny et al. [7]. The presence of a screw dislocation raises the solubility curve with respect to the homogeneous case, similarly to the edge dislocation case [9]. Consistently with the classical theory of heterogeneous nucleation [22], the interaction of the dislocation strain field with the solute atoms reduce the strain energy in presence of a precipitate embryo, hence decreasing solubility and catalyzing precipitation. The curve lies above the reactor working temperature, therefore below this temperature precipitates are expected to form in presence of the dislocation, in both FeNiMn and FeCuNiMn. The phases that precipitate inside the miscibility gap can be identified as mixed phases that contain bcc Mn, B2 phase NiMn, and (if the element is present) bcc Cu. The presence of Cu atoms decreases the solubility limit compared to the situation without Cu atoms. A detailed description of the precipitates is given in the next section.

3.2. Solute precipitation around the screw dislocation

3.2.1. FeNiMn and FeCuNiMn

In all cases studied in this work using the MD-MC technique, homogeneous and heterogeneous segregation around the dislocation core is observed at 300, 400 and 500 K. Fig. 3 (Fig. 4) shows the solute segregation at the dislocation for the alloy Fe-0.5%Cu-0.7% Ni-1.4%Mn (Fe-0.7%Ni-1.4%Mn) at 300 and 500 K. As is known, the elastic distortions for the screw dislocation contains no tensile or compressive components (hydrostatic pressure) and the stress field exhibits complete radial symmetry [23], thus there are no preferential sites for the different types of atoms, at variance with the results obtained for the edge dislocations [6]. As a consequence, solutes precipitate in a homogeneous fashion all around the dislocation line.

Besides the precipitation around the dislocation line, precipitates are also dispersed in the matrix, especially in presence of

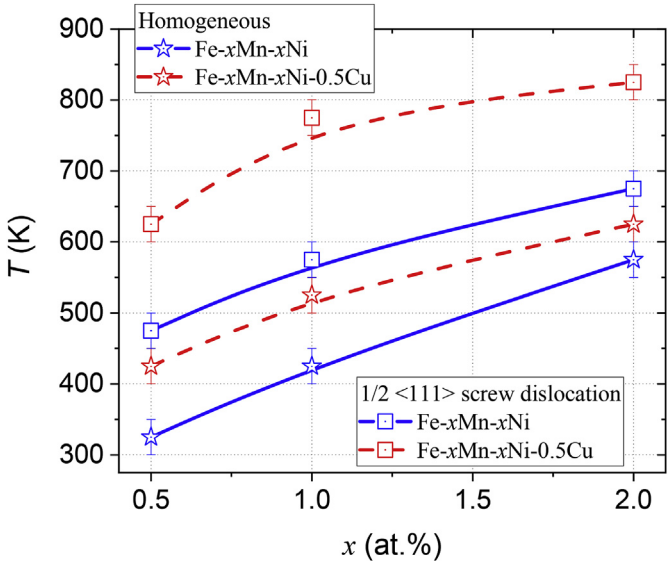

Fig. 2. Comparison of the NiMn and NiMn0.5%Cu solubility limit for defect free alloys and alloys containing a ½⟨111⟩ screw dislocation line. The concentration *x* denotes both Ni and Mn content, along the $x_{Ni} = x_{Mn}$ domain.

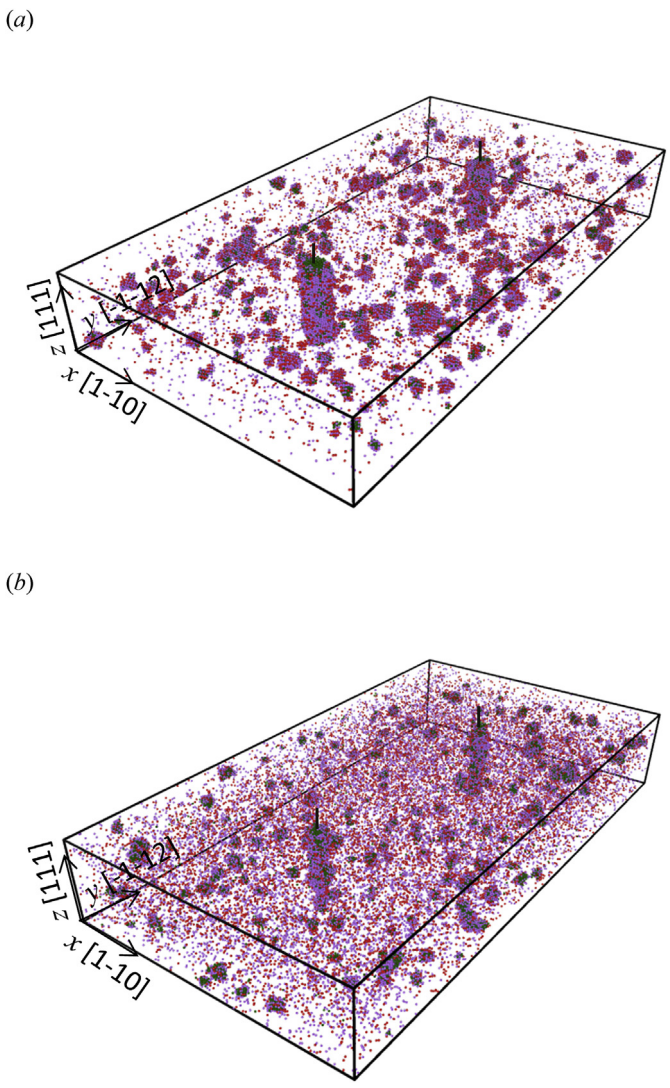

Fig. 3. Distribution of solutes in presence of a screw dislocation dipole for Fe-0.5%Cu-0.7%Ni-1.4%Mn alloy at segregation temperature: (*a*) 300K and (*b*) 500K. Ni atoms in red, Mn atoms in violet and Cu atoms in green. Dislocation lines are denoted by a black line. (For interpretation of the references to colour in this figure legend, the reader is referred to the Web version of this article.)

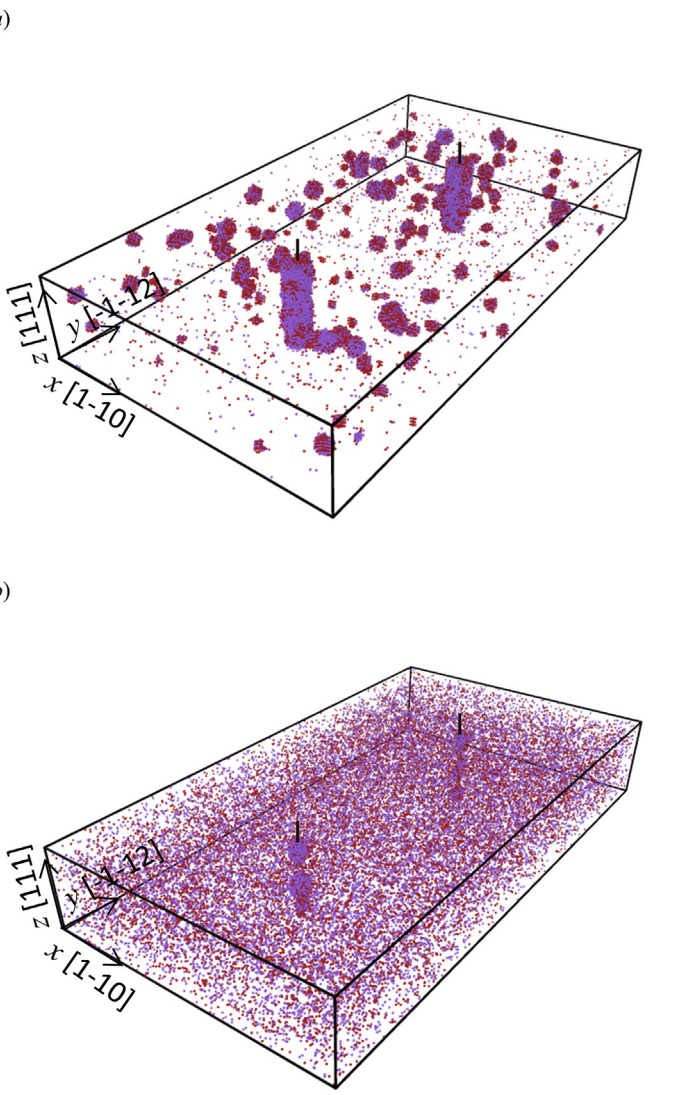

Fig. 4. Distribution of solutes in presence of a screw dislocation dipole for Fe-0.7%Ni-1.4%Mn alloy at segregation temperature: (*a*) 300K and (*b*) 500K. Ni atoms in red, Mn atoms in violet. Dislocation lines are denoted by a black line. (For interpretation of the references to colour in this figure legend, the reader is referred to the Web version of this article.)

Cu, except for the case of FeNiMn at 500 K, in which atoms segregate exclusively around the dislocation lines, without forming precipitates in the matrix. These results are fully consistent with, and could have been predicted by, the solubility curves of Fig. 2, at least for the cases with equal Ni and Mn content (1%Ni-1%Mn), with and without Cu. The cases with different content of Ni and Mn, as 0.7%Ni-1.4%Mn, however, could not be foreseen based on that figure. The quantity of segregated atoms that surrounds the dislocation generally decreases with increasing temperature, as should be expected because the higher the temperature the weaker the thermodynamic driving force towards precipitation; this is summarized in Table 1. This table reports, in particular, the fraction (%) of solutes segregated around the dislocation line, the composition (%) of the segregated region around the dislocation (%), the fraction (%) of B2 precipitates (%), and the percentage of the total volume fraction of precipitated phases around the dislocation line. In all cases the reference for normalization was the total amount of atoms in the box. An inspection of the table reveals that the element with the strongest tendency to segregate around dislocations is Mn, followed by Cu and then Ni.

The transversal *xz* section of the simulation box shown in Fig. 5 for representative cases studied at 500 K allows the solutes distribution around the dislocation to be appreciated. When the alloy contains more Mn than Ni, more Mn atoms segregate around the dislocation core. Ni atoms combine with Mn atoms forming the NiMn B2 structure, consistently with previous work [6,9] and with the preliminary study performed here to establish the solubility limit curve. The NiMn B2 phase surrounds the excess of Mn atoms. When Cu is present, Cu atoms form clusters, in competition with the B2 phase.

It is important to emphasize that these atomistic simulation results are supported by recent experimental observations obtained by examining irradiated RPV steel-type model alloys. In Fig. 6 we show a micrograph from an STEM-EELS study of neutron irradiated high CuMnNi model alloys, that contain Mn, Ni and Cu in proportions similar to those considered in this work [21]. When observed with atomic resolution STEM, the MnNi solute clusters have a BCC-like crystal structure. The corresponding chemical

Table 1
Summary of results after segregation at 300, 400 and 500 K: fractions of solutes segregated around the dislocation line, composition of the segregated region around the dislocation, volume fraction of B2 precipitates, total volume fraction of precipitated phases, maximum shear stress (MPa) obtained in MD simulations at 300 and 600 K and the elastic response.

Alloy	Temp. (K)	Precipitation round disloc. (%)	Composition of precipitates (%)			B2 fraction (%)	Total fraction (%)	Max. stress (MPa)	
			Cu	Ni	Mn			600 K	300 K
Fe-1%Ni-1%Mn	300	27.25	–	34.9	65.1	0.22	0.62	4493	5056
	400	23.21	–	30.4	69.6	0.11	0.47	3684	5088
	500	5.86		47.1	52.9	0.06	0.12	2099	2708
Fe-0.7%Ni-1.4%Mn	300	41.91	-	14.5	85.5	0.12	0.85	3754	4329
	400	43.56	-	7.3	92.7	0.08	1.05	3501	4576
	500	8.11		16.4	83.6	0.03	0.17	2336	3177
Fe-0.5%Cu-1%Ni-1%Mn	300	21.19	41.2	16.6	42.2	0.09	0.56	3643	4034
	400	23.40	18.3	15.5	65.8	0.08	0.54	3937	4767
	500	11.23	44.0	12.7	43.3	0.04	0.29	3518	4241
Fe-0.5%Cu-0.7%Ni-1.4%Mn	300	41.36	15.5	4.6	80.0	0.05	1.15	3447	5145
	400	34.42	5.2	9.2	85.6	0.07	1.08	3779	3842
	500	11.40	29.3	8.6	62.0	0.03	0.30	2517	3496

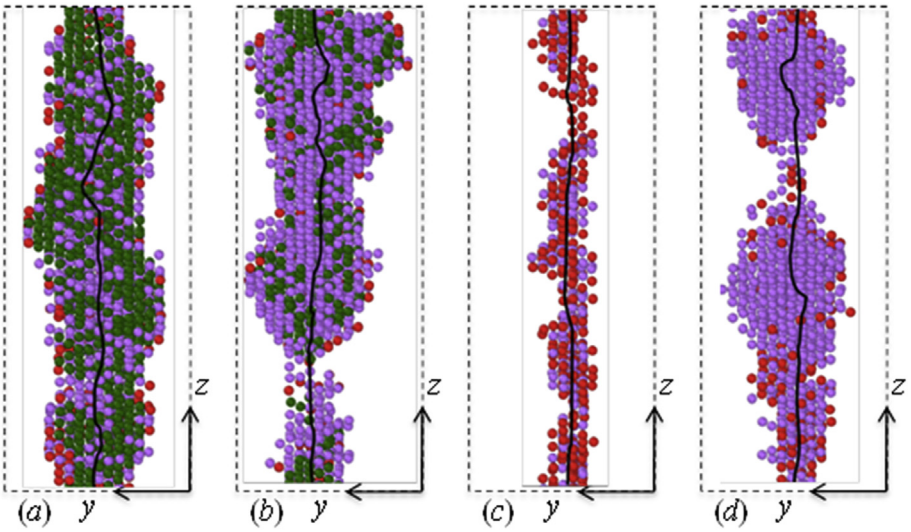

Fig. 5. Clusters sections (T = 500K) of representative examples on: (*a*) Fe-0.5%Cu-1%Ni-1%Mn, (*b*) Fe-0.5%Cu-0.7%Ni-1.4%Mn, (*c*) Fe-1%Ni-1%Mn, (*d*) Fe-0.7%Ni-1.4%Mn. Green atoms: Cu, red atoms: Ni, violet atoms: Mn. Dislocation line is in black). Box size: z = 10 nm, y = 3 nm. (For interpretation of the references to colour in this figure legend, the reader is referred to the Web version of this article.)

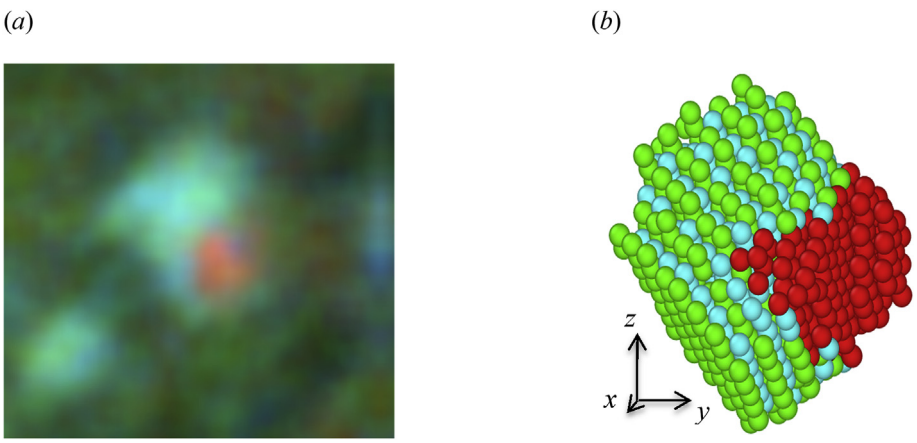

Fig. 6. (*a*) STEM-EELS micrograph showing what most likely is B2 phase with Cu appendage, (*b*) precipitate obtained by atomistic simulation where a qualitatively very similar feature was spontaneously produced: red spheres are Cu atoms, green ones are Ni and light blue ones Mn. Size: 2 nm. (For interpretation of the references to colour in this figure legend, the reader is referred to the Web version of this article.)

analysis [24] reveals that the observed microstructural feature corresponds most likely to a B2 precipitates with Cu appendage, in striking agreement with the result of the MMC simulation shown beside it, that also predicts the formation of the B2 MnNi phase on a dislocation, with a Cu precipitate appendage [21]. These complex solute clusters were often found in the experiment to be associated with dislocations. The average diameter of the experimentally observed MnNi solute clusters is 3.5 ± 0.5 nm, and 4.3 ± 0.5 nm for those with Cu appendages. Similar evidence of precipitation on dislocation under irradiation (in this case a $NiFe_3$ intermetallic phase in an Fe-3%Ni alloy) has been reported by Belkacemi et al. [4].

3.2.2. FeP

MD-MC simulations show also a strong segregation of P atoms to the core of the screw dislocation at 300 K. Here too, unlike the case of an edge character [6], the segregation is more homogeneous into the core, since no compressive or tensile sides exist. The binding energy of a single P to the dislocation core reaches $E_b = -2.3$ eV, i.e., much stronger attraction than in the case of the edge dislocation. Again, the binding energy was calculated as the difference between the energy of the system with a P atom at the most favorable site at the dislocation core and the energy of the system with the P atom in a region of the sample representative of bulk (i. e. far from the dislocation). Fig. 7 presents one half of the sample after the MD-MC simulations with a P concentration of 1.64 10^{-2}%, where we observe that all the P is segregated into the dislocation core.

3.3. Stress-strain curves

3.3.1. FeNiMn and FeCuNiMn

The simulation boxes where segregation was obtained around the dislocation dipole were divided in two parts, each containing only one dislocation. In all cases the proportion of segregated solutes is similar for both dislocations. As described in section 2, the dislocation unpinning stress was studied in these boxes at two temperatures, representative of tensile test temperatures of 300 K and 600 K. In Table 1 the maximum unpinning stresses are shown for the simulations using as initial state the segregation obtained at 300, 400 and 500 K, for all chosen alloys. A detailed comparison of the loading curves is presented in Fig. 8, for segregation temperature 500K, in four alloys: (*a*) Fe-1%Ni-1%Mn with and without Cu and (*b*) Fe-0.7%Ni-1.4%Mn with and without Cu. In all cases, consistently with expectations, the higher values correspond to the lower strain temperature, i.e., 300 K. The shape of the curves at segregation temperatures 300 and 400 K (not shown here) is very similar, only the unpinning stress values change.

As can be seen in Fig. 9, the values of the unpinning stresses increase with the total volume fraction of precipitated phases until a fraction of 0.8%; from there on the values decrease. This effect correlates with the amount of Mn atoms next to the dislocation. When the core is surrounded by Mn atoms the maximum stress values are lower, possibly because the Mn excess lowers the fraction of MnNi B2 ordered phase, suggesting that, as happens in the edge dislocation case, the B2 structure is indeed harder than bcc

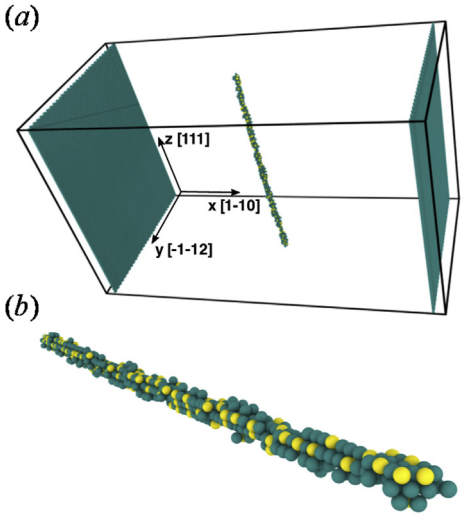

Fig. 7. Distribution of P atoms (yellow) in the presence of an screw dislocation in α-Fe (green). The P concentration is 0.0164%. (*a*) shows the box orientation with the dislocation and (*b*) displays a zoom into the dislocation core. (For interpretation of the references to colour in this figure legend, the reader is referred to the Web version of this article.)

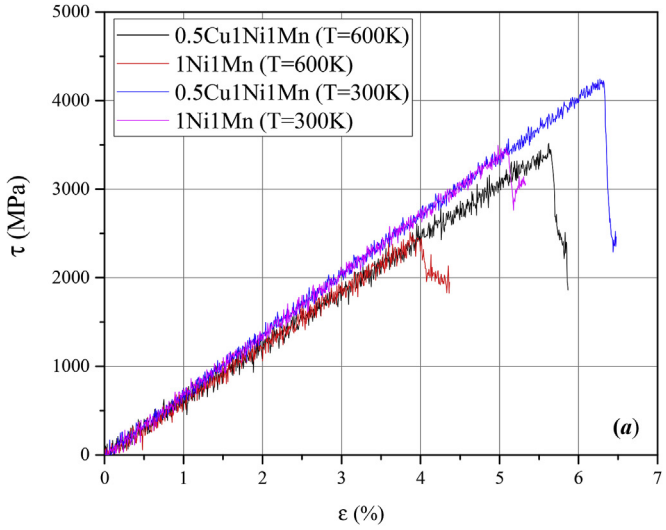

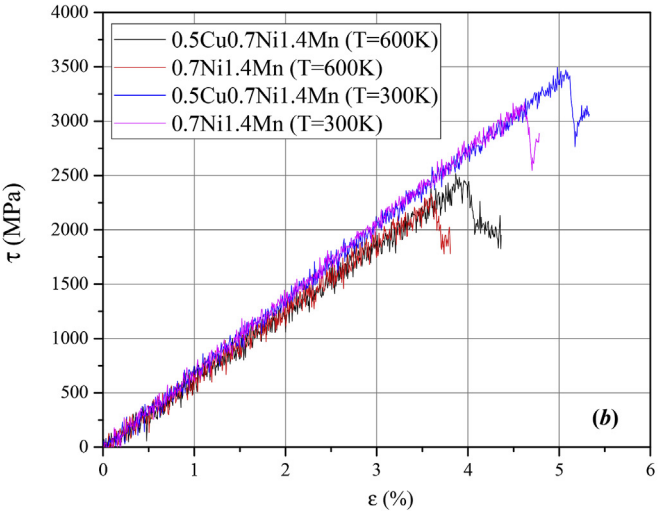

Fig. 8. Stress-strain curves for a screw dislocation in BCC Fe alloys with different solute concentrations after segregation occurred around the dislocation line at 500K: (*a*) Fe-1%Ni-1%Mn with and without 0.5%Cu and (*b*) Fe-0.7%Ni-1.4%Mn with and without 0.5% Cu. The temperatures at which the stress-strain curves were obtained (test temperature) are reported in the figures.

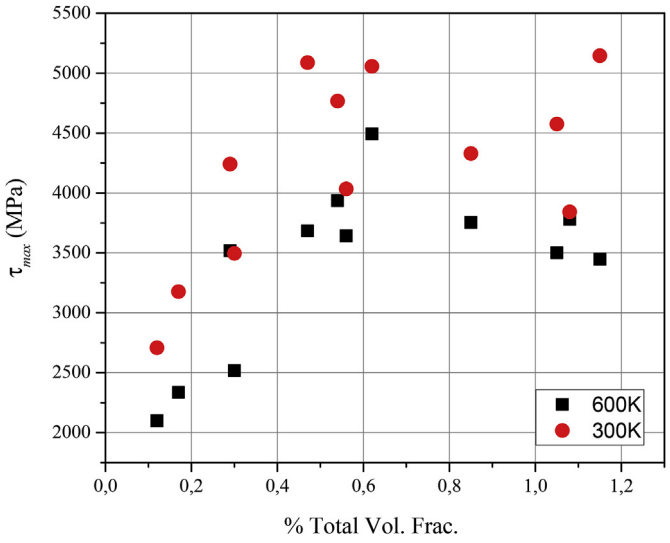

Fig. 9. Maximum stress vs. total volume fraction of segregated atoms (%) at the dislocation line. Squares (black) show results at 600K and circles (red) at 300K. (For interpretation of the references to colour in this figure legend, the reader is referred to the Web version of this article.)

Mn. For Fe-1%Ni-1%Mn and Fe-0.7%Ni-1.4%Mn obtained at 500 K, Fe atoms are located in the dislocation core, which may explain the lower unpinning stress.

To compare with a system without clusters, a reference curve (friction stress) was produced for different amounts of solutes dispersed in the matrix: 0.5%Cu-1%Ni-1%Mn, 1%Cu-2%Ni-2%Mn, 2% Cu-4%Ni-4%Mn, 4%Cu-8%Ni-8%Mn and 8%Cu-16%Ni-16%Mn. Only in the last case, which does not correspond to any realistic one, is the maximum stress significantly high, approximately 500 MPa; in all other cases the results are the same as in pure Fe [25].

3.3.2. FeP

The same methodology was followed to study the effect of P segregation on the critical resolved shear stress for the dislocation to overcome the solute pinning and start moving. A simple shear was applied to obtain the dependence of the yield stress on the P content (Fig. 10). Fig. 10*a* presents the stress-strain curves at 300K, which show a significant dependence on P concentration. Moreover, we note that the presence of P leads to remarkable hardening, significantly larger than in the case of the edge dislocation. This result is related to the stronger binding energy between the P and the screw dislocation. The slope of the yield point versus P concentration is related to this binding energy. We observe that the linear fit reproduces remarkably well the MD data for the whole concentration range explored in this work, as observed in Fig. 10*b*.

4. Discussion

Our results confirm that matrix dislocations, both edge [6] and screw, are preferential sites for segregation and thus subsequent nucleation of solute clusters and precipitates, because their presence locally decreases the solubility limit. This agrees with experimental evidence that has also been provided in this paper, where correspondence is found not only qualitatively (segregation and precipitation at dislocation lines), but also in terms of phases formed (B2 phase and pure Cu precipitate appendage). The hydrostatic component of the stress field, absent in the case of screw dislocations, is thus not a prerequisite for solute precipitation of substitutional solute atoms.

Given the large critical stresses obtained in Fig. 8, the mechanical consequences of this precipitation can be described in two ways: (*i*) unpinning of the matrix dislocations decorated by precipitates and (*ii*) interaction of the free dislocations with precipitates (heterogeneous and homogeneous distribution).

The first feature pertains to the onset of plastic deformation, inducing an upper yield stress (static aging) and Lüders plateau. For the edge dislocation, the critical shear stress τ_c necessary to unpin from decorating precipitates at 300 K is larger than 1 GPa [6] and the present results show that it is larger than 2.5 GPa for screw dislocations in all the investigated alloys. In order to assess the contribution of this threshold to the macroscopic flow stress, a rough estimation using the Taylor model for plastic deformation of polycrystals provides a yield stress $\sigma_y = M\ \tau_c$, with M being the Taylor factor (close to 2.7 [26] in BCC alloys). This means that, even when neglecting all other obstacles and the Hall-Petch effect, the upper yield stress must be at least equal to 2.7 GPa. Since the yield stress of heavily irradiated RPV steels never exceeds 1 GPa [27], this suggests that, under usual deformation conditions of irradiated RPV steels, the precipitate-decorated dislocations, such as those revealed in this work, remain immobile. Plastic deformation must thus only be carried by freshly generated dislocations, most probably from grain boundaries [28]. Once these dislocations are generated in a given material, they expand at large velocity. If the obstacle density (including dislocations) is small, then the stress drops because nothing hinders the dislocation motion after nucleation. This is indeed the case in annealed low carbon steels [29]. In irradiated RPV steels, the microstructure is characterized by a large dislocation density [30] and high density of solute clusters, thus the freshly generated dislocations will encounter a large

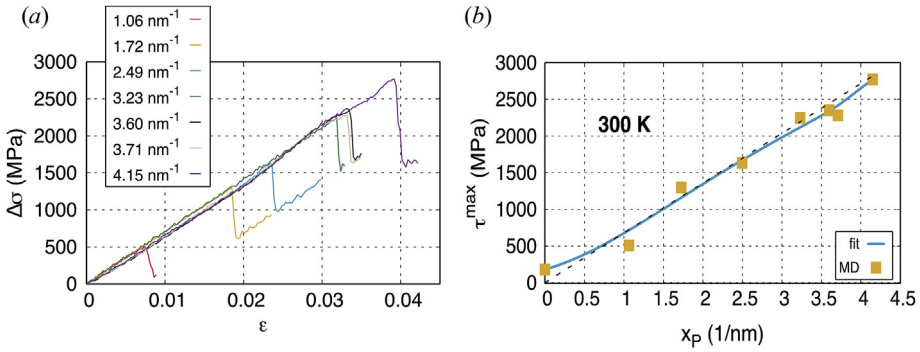

Fig. 10. (*a*) Stress-strain curves depending on the P content. (*b*) Yield stress versus P composition. Yellow points represent MD results and the blue line shows a spline fit. The dashed straight line displays a slope given by the binding energy of a single P atom to the screw dislocation. (For interpretation of the references to colour in this figure legend, the reader is referred to the Web version of this article.)

resistance, which explains the absence of strong upper yield stress at room temperature. In other words, it is reasonable to propose the following scenario for the yield stress in irradiated RPV steels: irradiation leads to precipitation in the bulk and also, importantly, decorating matrix dislocations, which become immobile. Plastic slip is thus carried by new dislocations. But the stress needed to generate these dislocations is of the same order of magnitude as the one needed for the new dislocations to shear the precipitates in the bulk, so no strong yield drop is observed.

The second feature can be investigated using the classical framework of precipitation hardening. However, in this framework the interaction statistics are given for a homogeneous (random) distribution of precipitates, while our results show that most of the precipitates are located on dislocation lines. It is thus necessary to assess the effect of the precipitate distribution on hardening, provided that the volume fraction V_f is kept constant.

In the case of random distribution, the newly generated dislocations interact with precipitates with a given density C and average size D, corresponding to a volume fraction:

$$V_f = \frac{\pi}{6} D^3 C \tag{1}$$

Dislocation dynamics simulations of precipitation hardening [31] have shown that the precipitation strengthening induced by the random distribution τ_{rand} can be given by:

$$\tau_{rand} = \left(\frac{\Omega_{pro} \mathrm{In}(2D/b)}{\Omega_{\infty} \mathrm{In}(l/b)} \right)^{3/2} \frac{\mu b \mathrm{In}(\mathrm{l/b})}{2\pi l} \approx \alpha \mu b \sqrt{DC} \tag{2}$$

where Ω_{prc} is the shear resistance of the precipitates, Ω_{∞} is a constant equal ~4.5 GPa, l is the average planar spacing between defects: $l = 1/\sqrt{DC} - D$, μ is the shear modulus (taken equal to 83 GPa [32]) and b the norm of the Burgers vector (equal to 0.248 nm). Usually, the average planar spacing is much larger than the precipitate size, which allows l to be expressed as $l = 1/\sqrt{DC}$. Since all other terms in eq. (2) involve logarithms of C and D, precipitation hardening scales, in a first approximation, as the square root of the planar density of the random distribution $\rho_{rand} = DC$, which is expressed in the approximation given in eq. (2).

In the present case of heterogeneous distribution, we can assume that all the precipitation occurs on the dislocation line. Of course, in our results we did not observe pure heterogeneous precipitation. This approximation helps, however, to investigate the asymptotic limit of hardening in the pure heterogeneous precipitation case. Instead of the spherical precipitates formed in a random distribution, we consider the precipitation to form a cylinder axed on the dislocation lines. For simplicity, we consider the diameter of the cylinder to be D. The linear density of such cylinders would be:

$$\rho_{heter} = \frac{4V_f}{\pi D^2} = \frac{2}{3}\rho_{rand} \tag{3}$$

Since the average planar spacing between cylinders is equal to $1/\sqrt{\rho_{heter}}$, precipitation strengthening induced by the heterogeneous distribution can be written as $\tau_{heter} = \alpha \mu b \sqrt{\rho_{heter}}$. Consequently the relation between the precipitation strengthening induced by the two distributions is given by:

$$\tau_{heter} = \sqrt{\frac{2}{3}} \tau_{rand} \approx 0.82\ \tau_{rand} \tag{4}$$

Within the assumptions made above, the precipitation strengthening in the case of complete heterogeneous distribution amounts to 82% of that induced by a full random distribution. Now, if we recall that, in most cases investigated in this paper, a significant amount of homogeneous precipitation is also observed, the difference in strengthening induced by the two distributions is even smaller. Consequently, when the precipitate diameter remains small, precipitation strengthening is little sensitive to the distribution. This important result suggests that eq. (2) can be indifferently used in the cases of homogeneous and heterogeneous distributions of precipitates.

5. Summary and conclusions

In this work we studied the formation and thermal stability of solute clusters near screw dislocations in FeCuNiMn and FeNiMn alloys. We found that solutes segregate and form mixed phase precipitates, that contain bcc Mn, B2 phase NiMn, and bcc Cu, in agreement with experimental observations reported in this same work. All phases precipitate mostly around the dislocation line, which effectively reduces the local solubility limit. The presence of Cu atoms decreases further the solubility limit compared to the situation without Cu atoms.

The results show that, when the fraction of Mn atoms increases to the detriment of the MnNi B2 phase, the critical stress to draw the screw dislocation out of the decorating precipitate decreases. This suggests that the shear resistance of the ordered MnNi phase is larger than that of a pure Mn coherent precipitate. The heavy segregation of solute atoms prevents the motion of the screw dislocation subjected to a stress lower than 2 GPa. This suggests that the initial matrix dislocations, when decorated, are in fact immobile in typical conditions of tensile tests. Deformation is accommodated by the motion of new, fresh dislocations, most likely generated from grain boundaries.

A simple geometrical analysis shows that precipitation strengthening is little sensitive to the precipitate distribution, homogeneous (random) vs heterogeneous (along dislocation lines).

In the case of P, we also see a strong segregation to the screw dislocation core, even stronger than for the edge character, proportionally to the stronger P-screw dislocation binding energy. This segregation considerably modifies the dynamical properties of the dislocation, increasing significantly the critical resolved shear stress that needs to be applied for the dislocation to be able to carry plasticity.

Acknowledgements

This project has received funding from the Euratom research and training programme 2014–2018 under grant agreement No 661913 (SOTERIA). This work also contributes to the Joint Program on Nuclear Materials (JPNM) of the European Energy Research Alliance (EERA). M.I. Pascuet thanks CONICET, Argentina and SCK•CEN, Belgium, for the accorded leave and hosting it, respectively. E. Martinez thanks LANL, an affirmative action/equal opportunity employer, which is operated by Los Alamos National Security, LLC, for the National Nuclear Security Administration of the U.S. DOE under contract DE-AC52-06NA25396.

Appendix A. Supplementary data

Supplementary data to this article can be found online at https://doi.org/10.1016/j.jnucmat.2019.04.007.

References

[1] C. English, J.M. Hyde, 4.05 radiation damage of reactor pressure vessel steels, in: Comprehensive Nuclear Materials, Elsevier, 2012.
[2] M.K. Miller, Russell, J. Nucl. Mater. 371 (2007) 145.
[3] M.K. Miller, K.A. Powers, R.K. Nanstad, P. Efsing, J. Nucl. Mater. 437 (2013) 107.
[4] L.T. Belkacemi, E. Meslin, B. Decamps, B. Radiguet, J. Henry, Acta Mater. 161

(2018) 61. https://doi.org/10.1016/j.actamat.2018.08.031.
[5] J.J.H. Lim, G. Burke, Private Communication.
[6] M.I. Pascuet, E. Martinez, G. Monnet, L. Malerba, J. Nucl. Mater. 494 (2017) 311.
[7] G. Bonny, D. Terentyev, A. Bakaev, E.E. Zhurkin, M. Hou, D. Van Neck, L. Malerba, J. Nucl. Mater. 442 (2013) 282.
[8] G.J. Ackland, M.I. Mendelev, D.J. Srolovitz, S. Han, A.V. Barashev, J. Phys. Condens. Matter 16 (2004) S2629–S2642.
[9] G. Bonny, D. Terentyev, E.E. Zhurkin, L. Malerba, J. Nucl. Mater. 452 (2014) 486.
[10] G. Monnet, D. Terentyev, Acta Mater. 57 (2009) 1416.
[11] R.G.A. Veiga, H. Goldenstein, M. Perez, C.S. Bequart, Scripta Mater. 108 (2015) 19.
[12] D. Terentyev, D.J. Bacon, Y.N. Osetsky, Phil. Mag. (2009) 1–15.
[13] D. Terentyev, L. Malerba, J. Nucl. Mater. 421 (2012) 32.
[14] G. Bonny, D. Terentyev, L. Malerba, J. Nucl. Mater. 385 (2009) 278.
[15] G. Bonny, D. Terentyev, L. Malerba, J. Nucl. Mater. 416 (2011) 70.
[16] E. Martinez, et al., Acta Mater. 84 (2015) 208–214.
[17] S. Plimpton, J. Comp. Physiol. 117 (1995) 1.
[18] B. Sadhig, P. Erhart, A. Stukowski, A. Caro, E. Martinez, L. Zepeda-Ruiz, Phys. Rev. B 85 (2012) 184203.
[19] J.P. Hirth, J. Lothe, Theory of Dislocations, McGraw-Hill, New York, 1968.
[20] Y.N. Osetsky, D.J. Bacon, Model. Simulat. Mater. Sci. Eng. 11 (2003) 427.
[21] J.J.H. Lim, M.G. Burke, Microscopy and Microanalysis 23 (S1), in: J.J.H. Lim, et al. (Eds.), "Microstructural Characterisation of Irradiation-Induced MnNi-Rich Solute Cluster in Highly Neutron-Irradiated MnNiMo Alloyed Weld Metals", 2013, ASTM International, West Conshohocken, PA, 2017, pp. 2198–2199.
[22] D.A. Porter, K.E. Easterling, Phase Transformations in Metals and Alloys, Springer-Science, 1992.
[23] D. Hull, D.J. Bacon, Introduction to Dislocations. Butterworth Heinemann, fourth ed., 2001.
[24] P.B. Wells, T. Yamamoto, B. Miller, T. Milot, J. Cole, Yu Wu, G.R. Odette, Acta Mater. 80 (2014) 205.
[25] C. Domain, G. Monnet, Phys. Rev. Lett. 95 (2005) 215506.
[26] J.M. Rosenberg, H.R. Piehler, Metall. Trans. 2 (1971) 257.
[27] A. Ulbricht, J. Böhmert, H.W. Viehrig, Microstructural and Mechanical Characterization of Radiation Effects in Model Reactor Pressure Vessel Steels, 2006.
[28] W.E. Carrington, D. McLean, Acta Metall. 13 (1965) 493.
[29] J.F. Butler, J. Mech. Phys. Solids 10 (1962) 313.
[30] M. Libert, C. Rey, L. Vincent, B. Marini, Int. J. Solids Struct. 48 (2011) 2196.
[31] G. Monnet, Acta Mater. 95 (2015) 302.
[32] G. Ghosh, G.B. Olson, Acta Mater. 50 (2002) 2655.